International Journal of Civil Engineering Applications Research (IJCEAR)
ISSN : 2249-653X
Vol. 4, No. 1, (2023), pp. 06-25

Finite Element Analysis and Optimization of Flexible Pavement

Atul Kumar Pandey[a], Deepak Mathur[b]
[a]M.Tech. Scholar, Department of Civil Engineering, KITE, Jaipur
[b]Associate Professor, Department of Civil Engineering, KITE, Jaipur
Email: atulkumarp59@gmail.com[a], mathurdeepak1507@gmail.com[b]

Article Received: 28 March 2023; **Revised:** 15 May 2023; **Accepted:** 10 June 2023

Abstract: This study explores the application of finite element analysis to parameter-sensitive analysis. The important performance parameters are investigated by altering the thickness and material characteristics of various layers of flexible pavement using a 2D axisymmetric analysis. Additionally, hypothetical pavement sections are examined in order to determine how sensitive the horizontal axisymmetric extension and mesh refinement are. Following validation, the generated computer programme is utilised to ascertain the impact of a single wheel load on the flexible pavement. The FEA analysis determines critical regions of pavement with maximum shear stress, maximum normal stress, total deformation, and stress intensity flexible pavement. The effect of different pavement layer thicknesses is then analyzed using the response surface method, and the numerical data is determined. The current design processes result in premature pavement breakdown or the construction of unprofitable pavement portions when the direct or indirect empirical approach is used. Applying experience, expert indentation, or a combination of both to the relationship between design inputs and pavement failure is restricted to a certain set of environmental and material variables. A good pavement design delivers the anticipated performance while taking into account the required economic factors, thus in this case it becomes necessary to discover a cost-effective option in the form of an analytical tool that can handle the specifics of the intricate pavement system. Instead of relying solely on CBR values, the use of such improved analytical tools can be advantageous for predicting the performance of pavement without actual construction or even by outperforming the costly and time-consuming laboratory or in situ tests, for various thicknesses and material properties of different component layers. In this regard, there is complete certainty in the use of the flexible finite element method (FEM) for the design of flexible pavement. The use of FEA for two-dimensional plane stress/strain and more rigorous three-dimensional finite element analysis for further extension of work is simple given that FEM is not restricted to two-dimensional axisymmetric conditions. By assuming equal stress states exist in every radial direction, axisymmetric modelling predicts pavement behaviour using a 2D mesh rotating around a symmetric axis; hence, loading is circular.

Keywords: *FEM, Pavement, CBR, FEA, 2D.*

1. INRODUCTION

There are two basic kinds of road pavements: Rigid & Flexible. Wearing surfaces on rigid pavements are typically made of Portland cement concrete, which functions like a beam across any imperfections in the supporting material. However, the bituminous materials used in flexible pavements ensure that even tiny abnormalities are kept in touch with the underlying substrate. A bituminous base is covered with a granular and a fine layer of material to create flexible pavements. Instead of using a foundation course, concrete pavements are constructed using Portland cement concrete.

There are four components to flexible pavements: the subsoil, the subbase, the base and the wear surface. The latter gets stiffer & contributes more to the pavement's strength when formed with Hot Mix Asphalt.

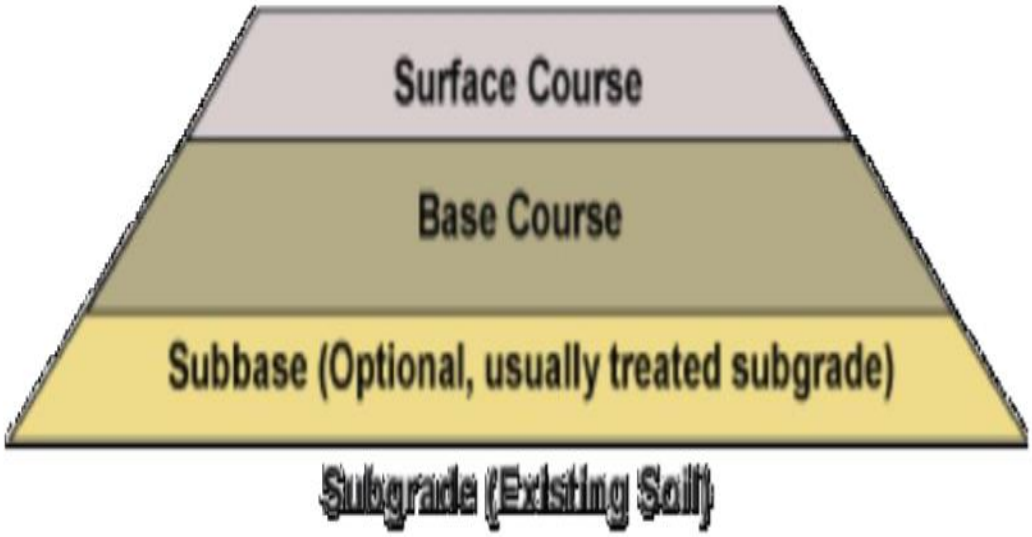

Figure 1.1: Schematic of a Flexible Pavement

1.5 Finite Element Method

It is advantageous to use the FEM approach to resolve mathematical equations in a variety of engineering contexts. It was suggested in the aerospace sector as a way to assess anxiety in challenging jet systems. It was embraced. This technique draws its inspiration from matrix analysis, which is utilised in the design of aeroplanes. Their individual fields of research have made significant progress. This method reduces the body's normal structural elements to "limited elements," which are finite-sized subcomponents. The variables connected to a small number of connections known as nodes or nodal points are studied in the initial frame and structure.

The assembly factor of the various joints, known as "nodal points" or "nodes," is taken into account in the analysis of the "limited element" if a model or component is divided into discrete portions termed "finite elements." The original construction or design is also taken into account. Since pressure and dislocation are components of an object's real change, the continuum does not recognise temperature, pressure, or velocity. A straightforward function can calculate the variation of the soil variable in a small area.

We might offer an interpolation model estimate function using the field node include method. If the field equations are constant, the nodal condition for a changing field is met.

After determining the nodal values, the field variable displays approximation traits throughout the element assembly process. There are still numerous issues with the finite element method that can be broken down into manageable pieces.

The following is an illustration of the method's step-by-step application to static structural applications:

Step 1: - Explanation of the Design Model (Domain). The final output area's structure is divided into smaller pieces or components using the finite element method.

Step 2: The appropriate interpolation technique was applied. We presume a reasonable conclusion in an unidentified solution component because the dislocation (field variable) explanation of a problematic structure cannot be anticipated accurately under all stress scenarios. Some union requirements must be completed, and the desired objective must be obvious.

Step 3: - The third step entails starting to create the inflexibility matrices for the components and load vectors. Both the predicted load vector P-load for the rigidity matrix (K(e)) and a suitable variant notion for rigidity matrices (K(e)) and the rigidity matrix load vector P-e should be employed in order to balance the rigidity matrices (K(e)).

Step 4: At this stage, equilibrium equations are constructed.

The various load vectors and firmness load vectors, as well as the overall equilibrium equation, are all stated in the same manner because there are multiple finite components.

$[K]\varphi = P$ Using a simple function, one may estimate the soil variable's variation in a constrained region.

If [K] is the mounted rigidity matrix, age is a nodal displacement vector, and a pressure vector, or nodal pressure, is known in its whole.

Step 5: - Using a system equation solution, you may find nodal displacements (subject variable). To take into account the limitations, it is required to alter the conventional equilibrium equations. Once the boundary conditions have been taken into account, the balancing equations can be given.

$[K]\varphi = P$

If the issue is linear, handling the vector " μ" will be simple. For non-linear problems, each step necessitates altering the firmness matrix (K) and responding to the or weight vector P in a series of stages.

Step 6:- To the nth power, stresses and strains are determined. From the supplied nodal displacements, the primary equations of stable or structural mechanics may be applied to derive detailed lines and stresses. The terms in parenthesis next to each of the procedures mentioned above relate to the FEM procedure that comes after it.

Objectives

This work main goal is to demonstrate the value of finite element analysis for analysing the impact of variations in important parameter thickness and material qualities, effect of single wheel load on flexible pavement. From the FEA analysis, critical regions of pavement having maximum shear stress, maximum normal stress, total deformation, and stress intensity's flexible pavement is determined. The effect of different pavement layer thickness is then analysed using response surface method, and the numerical data determined.

It is an attempt to correlate the results of the current study with actual field circumstances because the hypothetical thicknesses and material qualities that were taken into consideration for the analysis are typically employed in practise in accordance with IRC: 37-2012. Through this kind of examination, an equilibrium between weariness and rutting lives can be reached. The primary goal of the current study is to examine how the Response Surface Method optimisation technique affects the corner and edge stress created by pavement layer thickness.

1. CAD modeling of pavement using ANSYS design modelerwizard. Structural analysis on base design of pavement using ANSYS software.
2. Selection of optimization variables and conducting response surface optimization. These design points are width of different layers.
3. The DOE (design of experiments) table is generated and output parameters are evaluated for each design points generated. Generating sensitivity plot, 3d response surface plot and 2D response surface plot to aid in understanding the effect of each design variable.

2. LITERATURE REVIEW

Khan (1998) [1] The Group Index Method and the California Bearing Ratio Method are explored in relation to flexible pavement design. A soil's Group Index is used to estimate its thickness initially. Subgrade Group Index and thickness are presented in connection to different traffic conditions. Building depth and % of California Bearing Ratio Percentage are used in the construction of California Bearing Ratio curves.

Arora (2003) [2] Flexible pavement design strategies have been documented in a variety of ways. Methods such as McLeod's approach and the Group Index Method are among the many available. Thickness of foundation and surface are linked to traffic volume in Group Index Method constructions. Light, medium, and heavy traffic are plotted on CBR and pavement thickness curves in the CBR Method. The California Resistance Value Method employs the R-value, which stands for California Resistance. The Mcleod Method utilises graphs to show the relationship between construction depth and CBR under various traffic scenarios.

Punmia et. al (2005) [3] In this study, they report on the results of Burmister& elastic deformation analyses for flexible pavements. There have been produced charts for vertical deflections. Curves for the Group Index Method and the California Bearing Ratio Method have been made available for usage. This method uses the Group Index and the thickness of the line to plot the curves of the data. Using the California Bearing Ratio Method, a line is drawn from California Bearing Ratio to the thickness of a building's structure.

Subagio et.al (2005) [4] analyses the structural behaviour of many layers of pavement using approaches with an equivalent layer thickness. Multilayer pavement systems may be modelled using a one-layer pavement system

having identical thicknesses of one elastic modulus. The approach of equivalent thickness is based on the premise that the stiffness of a layer affects the stresses and strains that occur underneath it.

Das (2008) [5] Mechanisticempirical approaches to bituminous pavement design are discussed in this paper. The reliability of a certain pavement may be evaluated using a variety of failure criteria that take into consideration variations in pavement design input parameters. Based on empirical pavement design methods, a technique has been proposed to design asphalt pavements with a certain degree of overall dependability.

Tarefder et. al (2010) [6] The diversity of design inputs necessitates consideration of dependability in flexible pavement design. The dependability of flexible pavement designs and subgrade strength variations are examined in this research. The mean, maximum probability, median, coefficient of variation, & density distribution of subgrade strength are calculated. Both the dependability and thickness of the design outputs are taken into consideration when using these procedures. In terms of dependability, the AASHTO technique outperforms the probabilistic approach. Finally, altering the hot mix asphalt qualities are used to test the resiliency of the flexible pavement design. To alleviate various problems, it is suggested that the present pavement thickness be modified by altering the material and subgrade qualities.

Rahman et. al (2011) [7]Flexible pavement design often makes use of empirical methods like layered elastics and two-dimensional finite elements. More mechanical approaches are being used to lower the restrictions on stress, strain and displacement calculations for pavements nowadays. In order to achieve the study's requisite accuracy and convergence, researchers employed ABAQUS software to experiment with model size, element kinds, and meshing processes.

Ameri et. al (2012) [8]Pavements have been studied and designed using finite element analysis. Using the finite element approach, it is possible to investigate stability, time-dependent issues, and material nonlinearity. The Finite Element Method and the Theory of Multilayer System have both been used to examine a large number of common pavements in this work. As a consequence of this statistical study, the significance parameter and correlation coefficient were used to compare the findings of these two methodologies.

Finite-element analysis findings are best compared to those from the theory of multilayer systems in this research, and there is no significant difference in mean values between both.

Jain et. al (2013) [9]the design methodologies that have been historically used and the cost analysis for each type of rigid and flexible pavement design are discussed. Since they can be reinforced and upgraded incrementally as traffic increases, flexible pavements outperform cement concrete roads in terms of durability and their surfaces may be milled and recycled for rehabilitation. The initial investment and ongoing maintenance costs are lower with flexible pavement as well. Rigid pavement may be more expansive, but it requires less care and has a longer useful life. Flexible pavements have been shown to be more cost-effective for low-volume traffic. Flexible pavement has a life expectancy of around 15 years, however it requires regular maintenance after a given amount of time and the prices are quite expensive. More than 2.5 times as long as the 40-year life span of a flexible pavement, the life of rigid pavement is more than twice as long as that of flexible pavement.

Dilip et.al (2013) [10]In designing flexible pavements, consider the uncertainty associated with things like material qualities and traffic characterization. As a result of this, there have been major attempts in recent years to include dependability and probabilistic design approaches into pavement design, rehabilitation and maintenance. The first- and second-order reliability methods, as well as a rudimentary Monte Carlo simulation, are used in this work to assess the resiliency of a flexible pavement segment. Narrow boundaries are also recommended, since they offer a more accurate assessment of the failure probability, as shown by the Monte Carlo Simulation findings.

3. METHODOLOGY

3.1 Overview

An object, such as the cylinder depicted in Figure 3.1, is broken down into a series of discrete elements linked at their nodal points for finite element analysis. Nodal stiffness is determined for each element based on an assumed variation in element displacements and stress-strain characteristics of its material. Nodal point forces may be expressed in terms of nodal point displacements and stiffnesses for each nodal point in the system. The resulting equations are then used to determine the actual velocities. The strains and stresses in each element are then calculated based on the displacements of all nodal points. Real-world systems analysis often necessitates

the simultaneous formulation and solution of hundreds of equations. As a result, this method can only be used with modern, high-performance digital computers. The digital computer software that was employed in this investigation is detailed elsewhere. " In order to accurately reflect the behaviour of granular base and cohesive subgrade materials under traffic-like circumstances, modifications have been made to automatically produce acceptable finite element configurations for axisymmetric pavement structures analysis.

This computer application uses quadrilaterals and/or triangles to break down the structure to be studied. For the sake of this investigation, only quadrilaterals were used. The computer algorithm then divides each quadrilateral into four triangles. Within each triangle, the displacements are supposed to fluctuate linearly. This assumption guarantees the deformed structure doesn't develop gaps and that displacements are compatible all over and at all nodes. Each node's load or displacement and the material parameters of each element (Young's modulus and Poisson's ratio) must be specified in addition to the finite element configuration. The density of each material has to be supplied in order to determine the initial gravity stress (corresponding to no applied weight on the pavement) for each element in the nonlinear analysis. Nodal displacements at each of the quadrilateral components' nodal points, as well as a full state of stress at the centroid of each quadrilateral, are generated by the computer. The average of the stresses in the four triangles is used to calculate quadrilateral stresses.

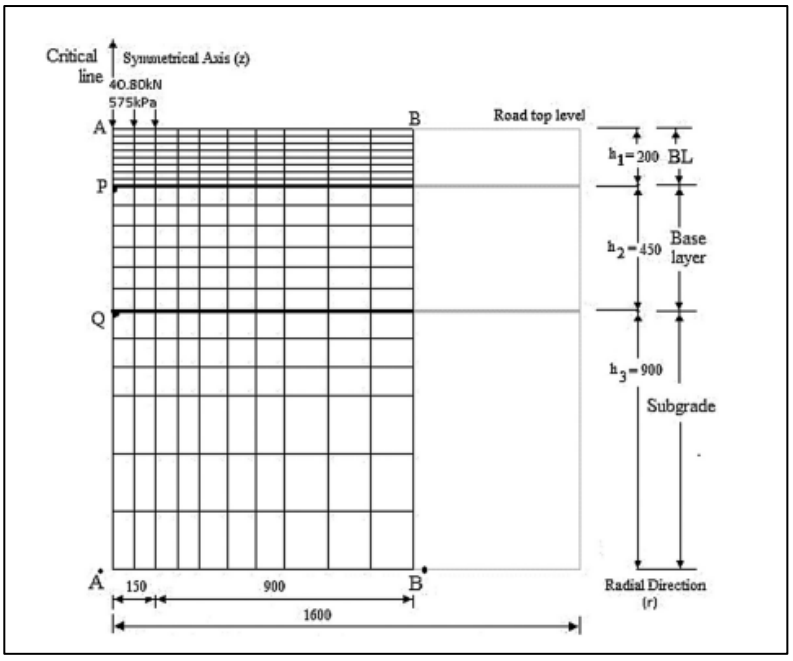

Figure 3.1: Pavement Section Showing Critical Line and Hypothetical Idealization

3.2 Methodology Steps

The analysis of pavement is conducted using techniques of FEM. Different stages of FEM are discussed in this section.

3.2.1 CAD Modelling

ANSYS design modeller is used to create the pavement CAD model. Figure shows the CAD model of the pavement that was produced.

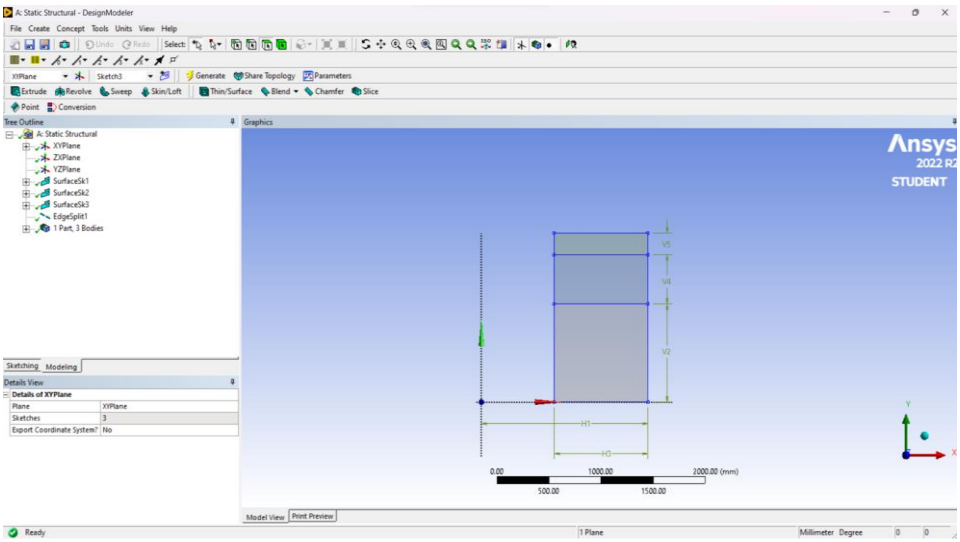

Figure 3.2: CAD Model of Pavement

The layer highlighted in figure 3.2 above comprises of wearing course and binder course.
The next layer is shown in figure 3.3 below which is base layer and sub base layer.

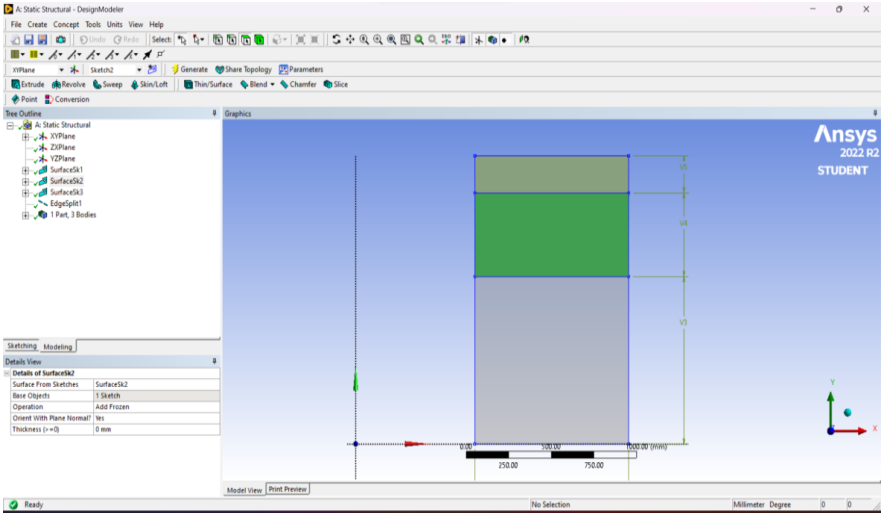

Figure 3.3: CAD Model of Pavement Base Layer

The bottommost layer of pavement is subgrade layer as shown in figure 3.4 below.

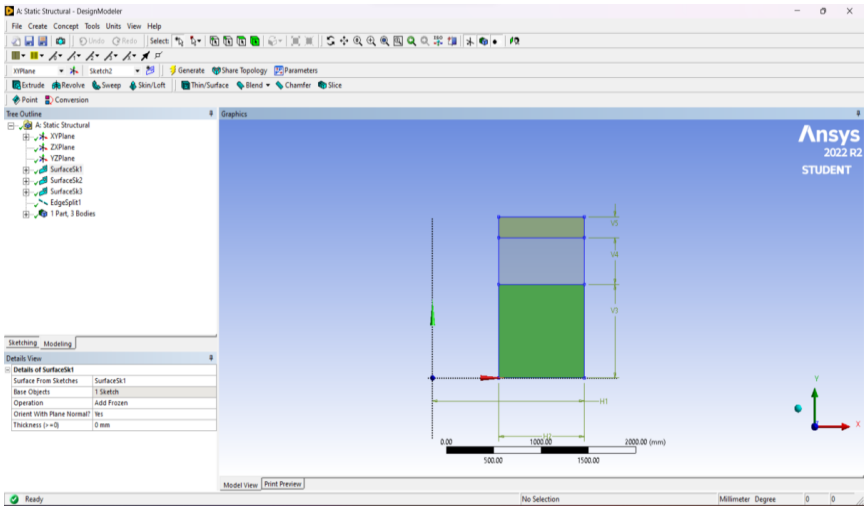

Figure 3.4: CAD Model of Pavement Subgrade

3.2.2 Meshing CAD Modelling in ANSYS

After CAD design of pavement is developed, it is meshed using hexahedral elements. The total number of elements and nodes created is 2232 and 7039, respectively. Due to topological consistency the model is suited for hexahedral elements.

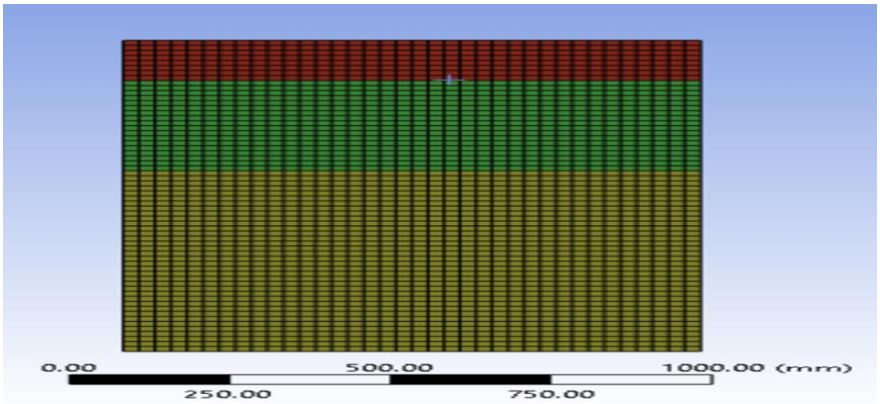

Figure 3.5: Hexahedral Element Meshed

3.2.3 Applying Loads and Boundary Conditions

Loads and boundary conditions are utilised in combination with the CAD model to provide force and displacement support.Depending on literature, there are a lot of restrictions. Pavement subbase is applied using a fixed support system.The loading condition are applied as per Indian Road Congress (IRC: 37-2012).

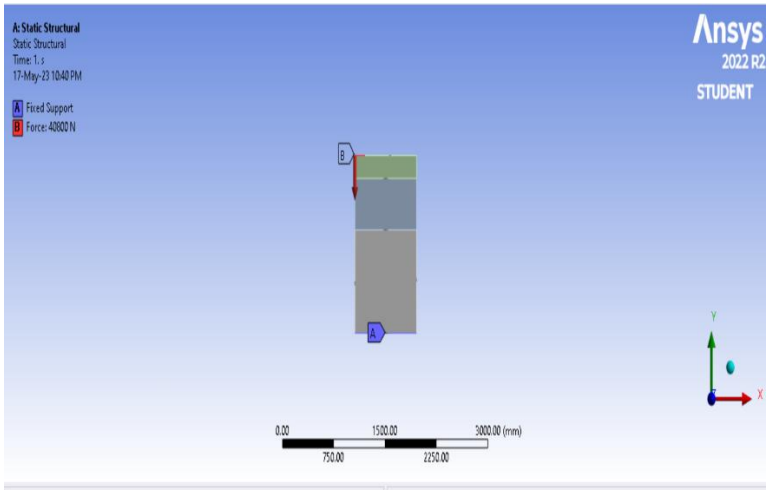

Figure 3.6: Loads and Boundary Condition

3.2.4 Solution Stage

At this stage, the stiffness matrix is formulated for each element type. The nodal calculations are made for deformation and stresses. The complete edge length of the element was interpolated in order to arrive at these findings.

3.2.5 Response Surface Methodology for Design Optimization

There are numerous methods in the response surface method (RSM) that may be used to analyse issues in which several independent variables have an impact on one dependent variable.[28]. There's a goal here: to maximise this reaction. When X1 is denoted as an independent variable, it is assumed to be continuous and controlled by the researcher with small error. Xn is the number of independent variables.[29]. To express the link between a dependent variable and one or more other variables, correlation may be used.

$$y = f(X_1, X_2, X_3, X4 \ldots\ldots X_n) + \varepsilon$$

The "y" answer has a "noise" or "error" in it.

The expected answer may be labelled as follows:

$$E(y) = f(X_1, X_2, X_3, X4 \ldots\ldots X_n) = \eta$$

This is referred to as the "surface"

$$f(X_1, X_2, X_3, X4 \ldots\ldots X_n) = \eta$$

is called the response surface[29].

The optimization parameters selected for optimization are shown in table 3.1 below.

Table 3.1
Optimization Variables

Subgrade	900mm
Baselayer	450mm
Bl	200mm

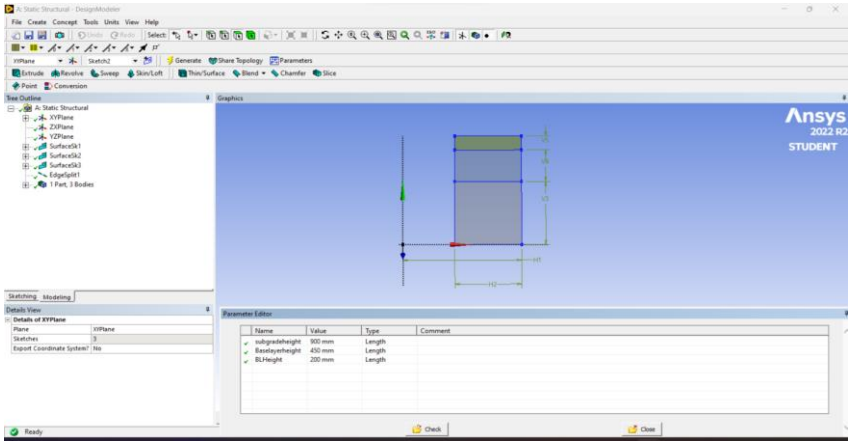

Figure 3.7: Variable Definition for Optimization

3.3 Optimization Types used for Research

3.3.1 Central Composite Design

Second-order response models are often employed in combination with these sorts of designs. As you can see, there are three sorts of points in this design.

1. Axial Points: A screening analysis generates axial points.
2. Cube Points: 2n cube points are derived from the total number of professors on a certain campus.
3. Center: A nominal design is used to generate a single centre.

The control parameter ranges (minimum and maximum values) are altered to [-1, + 1] for a more complete explanation of the diagrams. Central Composite (CCC) is used to create a three-dimensional design with a confined area. The axial points are located in a bi-radius hypercube. The lateral length of the cube formed by the cube points is 2.

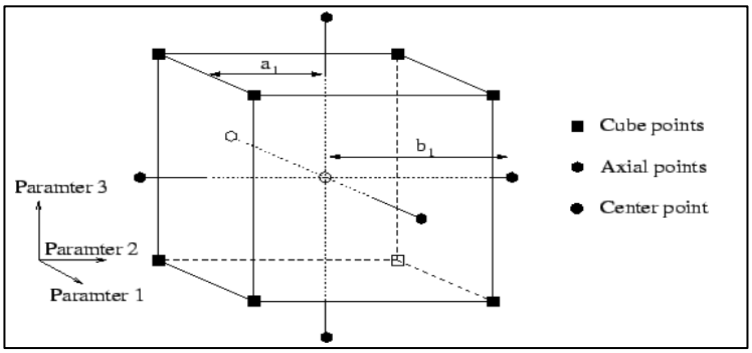

Figure 3.8: The Example Points of a *Central Composite Circumscribed* Design with Three Input Parameters

3.3.2 Optimal space filling design

Using deterministic models, it is preferable to employ space fill designs since the design points are uniformly distributed over the design area. There must be a computer simulation that accurately represents the physical system in order to employ these design choices. This article does not explore the ability of space fill designs to verify a simulation with physical test data, but rather illustrates how these designs are employed in a validated simulation to characterise a physical system.

These projects may record diverse reactions in different places due to the diffusion points. The response behaviour in the design space might alter dramatically according to the complexity of these simulations. In general, attempts to fill empty space strive to avoid making duplicates in as many dimensions as possible. The optimum space fill design does not contain replication points in the smallest design space when searching for elements that do not have a statistical influence on the response. As an example, when one element is found to be insignificant and the plan is projected onto the lowest dimension of the other factors, there is no reaction. Due to the deterministic nature of the result and the lack of extra information provided by the duplicated test points, this method allows us to learn more about the system in question.

1. Traditional DOEs (like CCD) would concentrate on modifying parameters near to the scope of the design area due to the noise involved with physical testing.
2. This restriction does not apply, or does not apply as much, to the computer simulation.
3. An equitable distribution of the design parameters is made possible by a room filling system.
4. The goal is to convey the most information possible with the fewest points.
5. The user can define the number of points, which is quite helpful when the available calculating time is constrained.
6. The design room's cover is not consistent. Centres and/or angles are not always included.
7. The choice of the beginning place takes into account a few risks.

Optimal space filling design is shown in figure 3.9

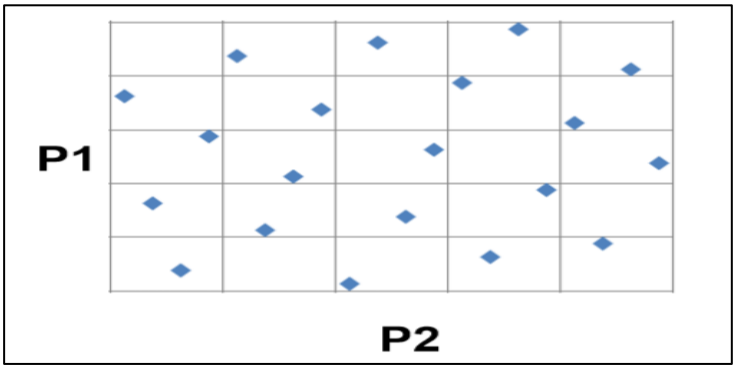

Figure 3.9: Optimal Space Filling Design

- **Benefit:** - provides the user with the option to define the number of design points. - You must enhance the functions that fill the available space if you wish to apply a more sophisticated metamodeling technique like kriging, non-parametric regression, or neural networks.
- **Disadvantage:** - Choosing too many design points can lead to poor response prediction quality since the ends are not always covered.

3.3.3 Box Behnken Design

The Box-Behnken layout lacks an integrated factorial or fractional layout and is a standalone square design. In this layout, the middle and edges of the treatment room are where treatment combinations are located. These designs can rotate (or virtually rotate) for each factor. The structures orthogonal to the main composite components can only be partially locked.

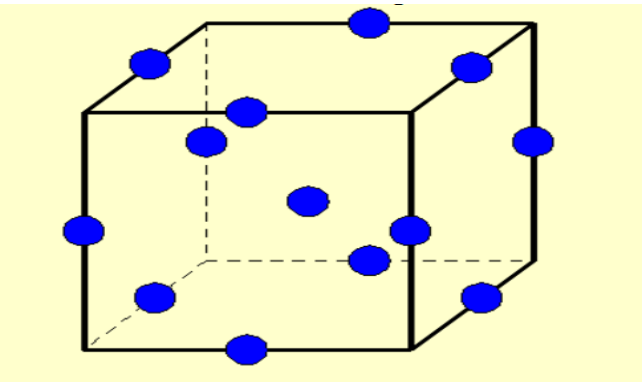

Figure 3.10: Box-Behnken Design for Three Factor

Projects developed according to the Box-Behnken method have processing combinations that "lie in the centre of the test room's edges and need at least three continuous components." A three-factor box barrier design is shown in the illustration below. These designs enable rapid estimation of the first and second order coefficients. Box-Behnken designs frequently contain fewer design points than central composite designs with the same number of pieces, so they might be less expensive to build. They are not suited for subsequent trials since they do not have an integrated factorial design. If we are aware of the process's safe operating area, using Box Behnken projects is also a possibility. Axial points are typical in core composite constructions outside of the cube. These locations might not be of local interest or might not be reachable due to being outside of the safe operating parameters. You may be sure that every design point in Box-Behnken projects is within the spectrum of safe operation. The Box-Behnken designs are employed to avoid this.

3.3.4 Sparse grid initialization

This approach was initially designed to solve partial differential equations. Smolyak, a Russian mathematician, is credited with introducing the basic concept of sparse grids. Hyperbolic crosses, Boolean techniques, discrete blending methods, and splitting extrapolation methods are also strongly connected to the notion. The sparse grid technique uses O (hn-1.log(hn-1)d-1 grid points in the discretization process to represent a function f defined across a d-dimensional domain, where hn:= 2n is the mesh size and n is the discretization level. O (hn2.log(hn-1)d-1 for an accuracy of O) may be proved to be the order of approximation for a function f given certain smoothness requirements (hn2). Sparse grids, on the other hand, need many fewer points in higher dimensions to obtain the same approximation quality as ordinary complete grids. The complete grid method's dimensionality curse is less severe for sparse grids, and these grids may be utilised to solve problems with larger dimensions.

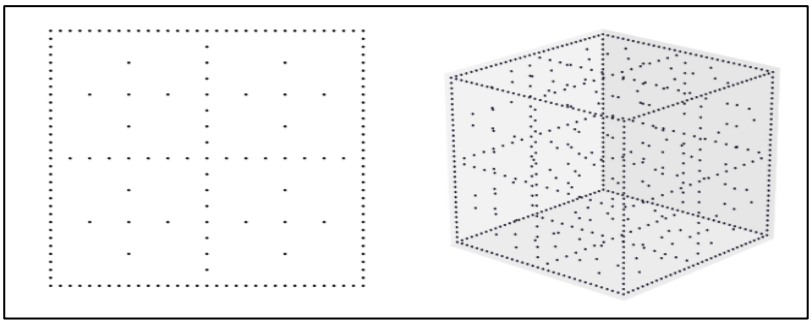

Figure 3.11: 2D Sparse Grid and 3D Sparse Grid

3.3.5 Latin Hypercube Sampling

There are just a few iterations in the latin hypercube sampling and the input probability distributions are stratified. In probability theory, stratification is the process of dividing the cumulative curve into equal intervals (0 to 1.0). Each interval or stratum of the input distribution is then randomly sampled. As a result, sampling is compelled to re-create the input probability distribution".

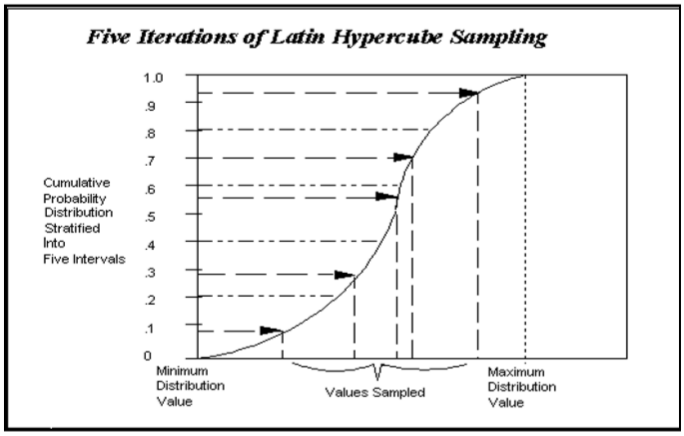

Figure 3.11: Latin Hypercube Sampling

The cumulative curve in figure 3.12 above is divided into five intervals using the Latin hypercube, which more precisely reflects the value distribution without replacement. Stratification affects the iteration numbers. The

sampling effectiveness and runtimes of the Latin Hypercube are considerably enhanced. Latin Hypercube analysis may be useful for probability distributions that contain low-probability events. Latin Hypercube sampling pushes the sample to include the outlying occurrences, ensuring accurate representation in your simulation findings.

4. RESULT AND DISCUSSION

4.1 FEA Results on Pavement

Normal stresses are determined using a FE study of pavement. The greatest horizontal normal stress is 0.026653 MPa, as illustrated in the red-colored zone. The normal stress is maximum at the point of load application which reduces along the downward direction.

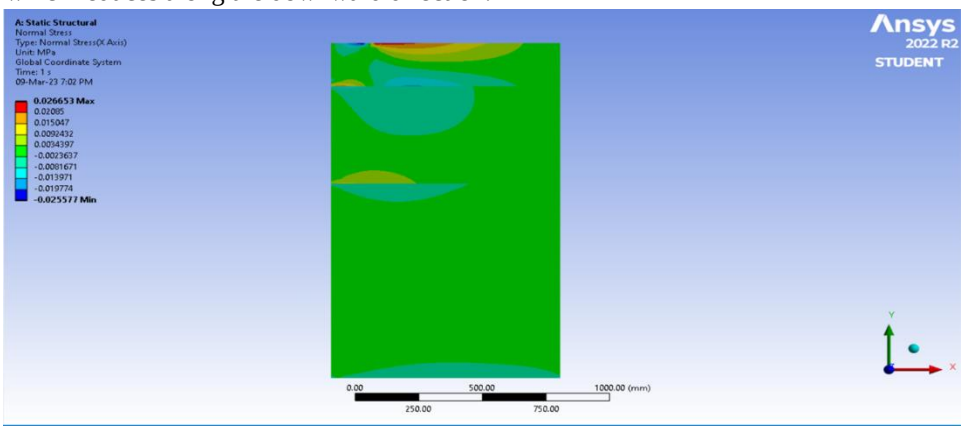

Figure 4.1: Maximum Normal Stress Along X Direction (Horizontal Direction)

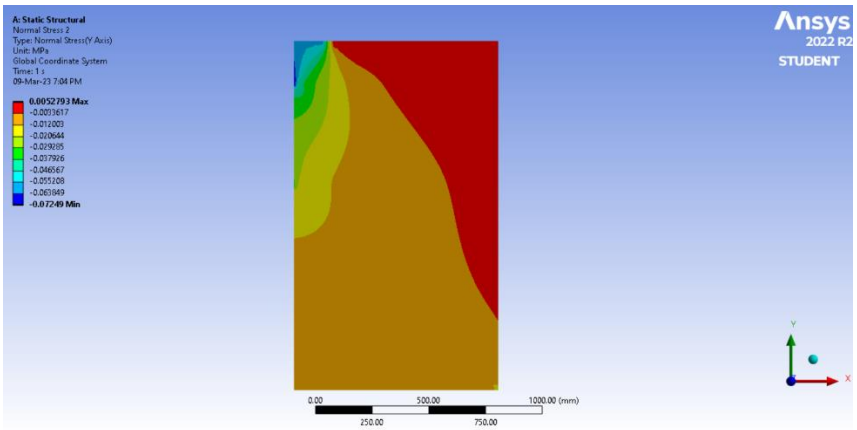

Figure 4.2: Maximum Normal Stress Along Y Direction (Vertical Direction)

Figure 4.2 shows the maximum normal stress in the vertical direction. The maximum normal stress is observed at the zone of load application with magnitude of 0.0052793MPa as shown in dark blue coloured zone. The normal stress reduces as we move towards the bottom region of pavement.

Maximum Normal Stress Intensity: The normal stress intensity plot is obtained from the FEA analysis of pavement. The maximum stress intensity is obtained at the corner region with magnitude of 0.084808MPa which reduces towards the bottom region and at the other free end.

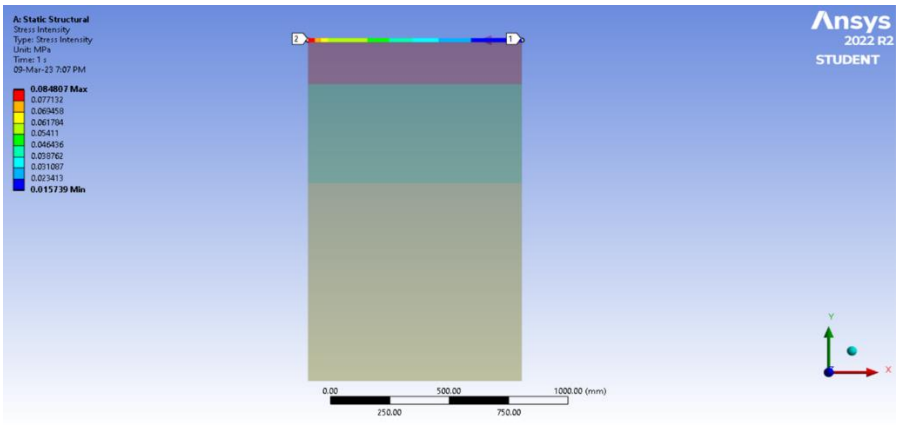

Figure 4.3: Maximum Normal Stress Intensity

Total Deformation Plot: The total deformation plot is obtained from the FEA analysis and the maximum deformation obtained from the FEA analysis is 0.13788mm at the point of load application which reduces towards the base of pavement and at the free end of pavement.

Figure 4.4 depicts the variance in total pavement deformation across its length. At the point where the load is applied, the overall deformation is greatest.

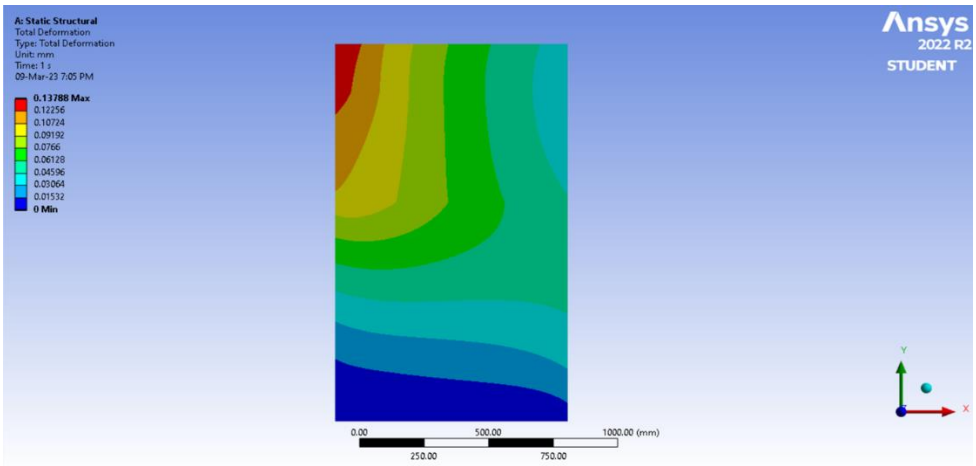

Figure 4.4: Total Deformation Plot across Length

4.2 Response Surface Optimization

The DOE table is generated from Taguchi response surface optimization method. It includes the optimization variables i.e., subgrade, baselayer, and bituminous layer. The output parameters include normal shear stress, normal stress, total deformation. We use a linear regression model to create the design points.

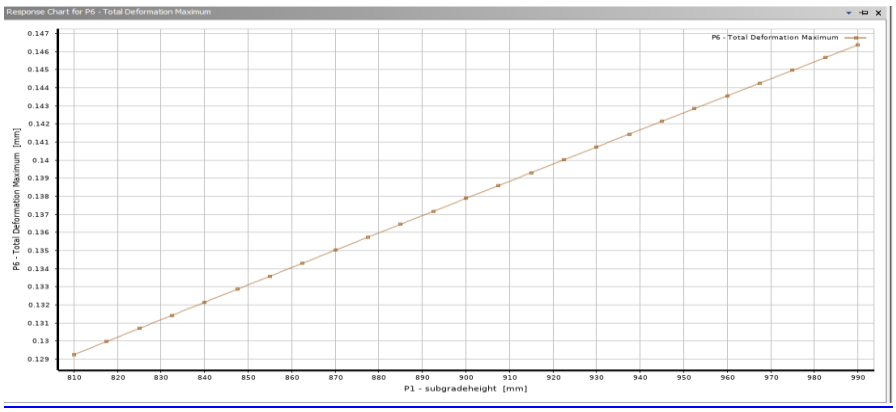

Figure 4.5: Normal Stress along Length

Table of Outline A9: Design Points of Design of Experiments

	A	B	C	D	E	F	G	H
1	Name	P1 - subgradeheight (mm)	P2 - Baselayerheight (mm)	P3 - BLHeight (mm)	P5 - Maximum Shear Stress 2 Maximum (MPa)	P6 - Total Deformation Maximum (mm)	P7 - Stress Intensity Maximum (MPa)	P8 - Normal Stress Maximum (MPa)
2	1 DP	900	450	200	0.042403	0.13788	0.084807	0.026653
3	2	810	450	200	0.0418	0.12925	0.0836	0.026835
4	3	990	450	200	0.042937	0.14637	0.085873	0.026494
5	4	900	405	200	0.043422	0.14103	0.086843	0.026344
6	5	900	495	200	0.041425	0.1351	0.08285	0.026966
7	6	900	450	180	0.043224	0.14061	0.086183	0.027001
8	7	900	450	220	0.041781	0.13552	0.083562	0.02627
9	8	826.83	413.41	183.74	0.043241	0.13552	0.086482	0.026689
10	9	973.17	413.41	183.74	0.044231	0.14984	0.088461	0.026394
11	10	826.83	486.59	183.74	0.042716	0.13076	0.0834	0.02717
12	11	973.17	486.59	183.74	0.042706	0.14454	0.08518	0.026896
13	12	826.83	413.41	216.26	0.042229	0.13112	0.084458	0.026325
14	13	973.17	413.41	216.26	0.043191	0.14518	0.086382	0.026045
15	14	826.83	486.59	216.26	0.040638	0.12678	0.081276	0.02683
16	15	973.17	486.59	216.26	0.041495	0.14033	0.082991	0.026572

Figure 4.6: DOE Table Generated

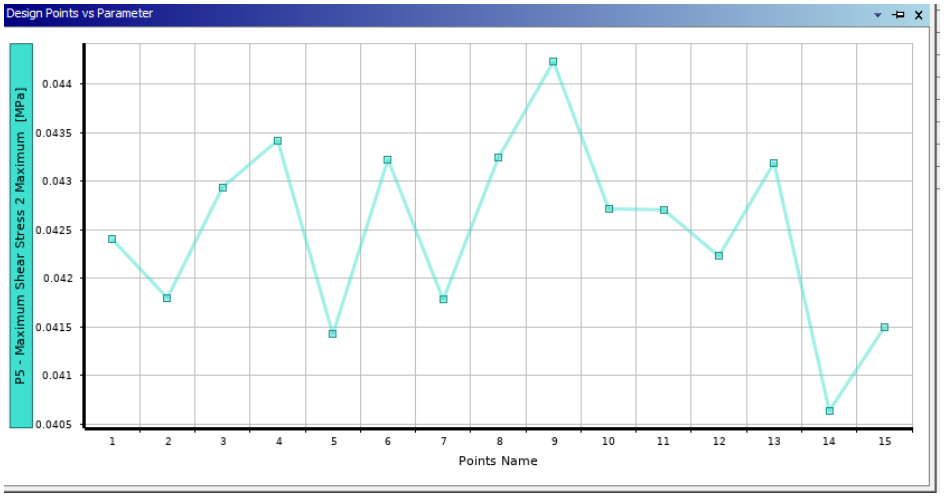

Figure 4.7: Shear Stress v/s Design Points

As its evident from figure 4.7 above, the minimum shear stress is obtained for design point number 14 which has dimensions of 826.83mm subgrade and 486.59 base layer and 216.26mm bituminous layer.

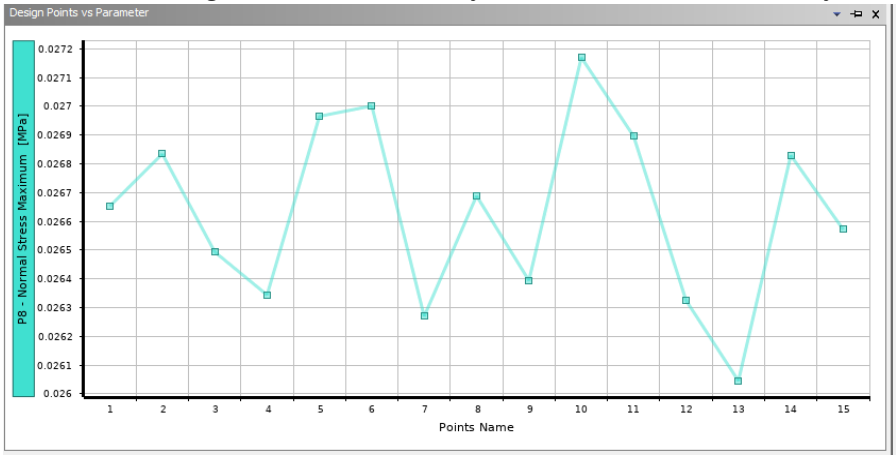

Figure 4.8: Normal Stress v/s Design Points

As its evident from figure 4.8 above, the minimum normal stress is obtained for design point number 13 which has dimensions of 973.17mm subgrade and 413.41mm base layer and 216.26mm bituminous layer.

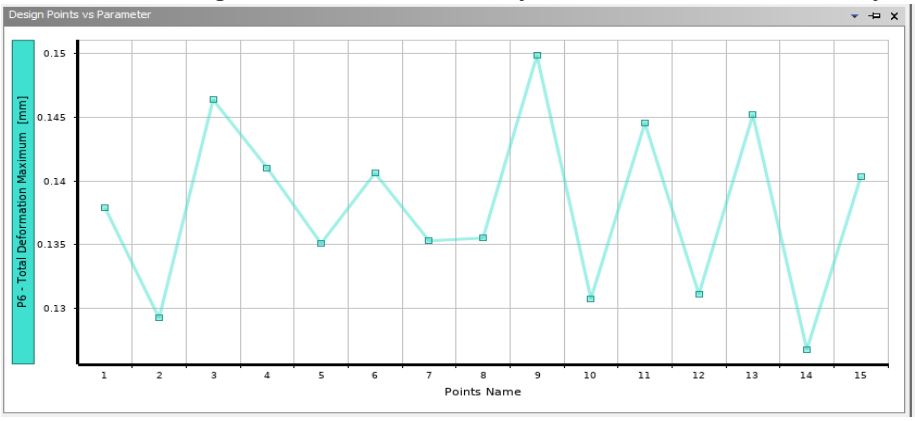

Figure 4.9: Total Deformation v/s Design Points

As is evident from the figure above, the minimum total deformation is obtained for design point number 14 which has dimensions of 826.83mm subgrade and 486.59 base layer and 216.26 mm bituminous layer, and maximum deformation is observed for design point number 9 (0.14897 mm).

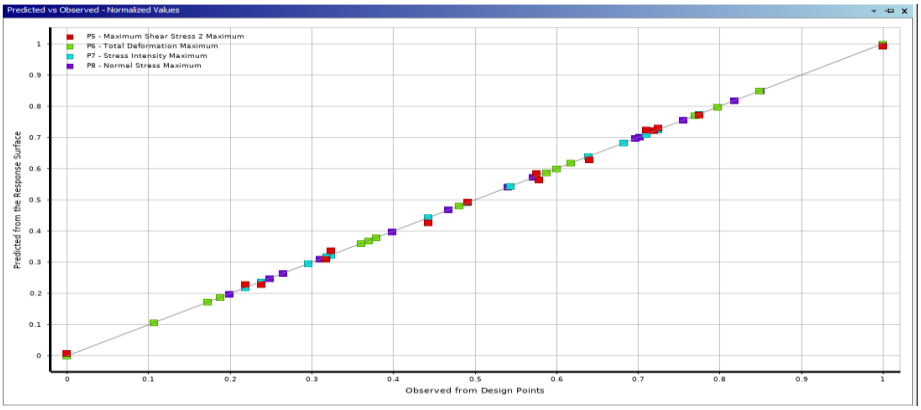

Figure 4.10: Goodness of Fit Curve

The solution yields a goodness-of-fit curve, which demonstrates the precision with which the DOE solution was arrived at. From the current solution, it is evident that very little deviation is observed for obtained values (represented in boxes) as compared to expected values (as represented in line).

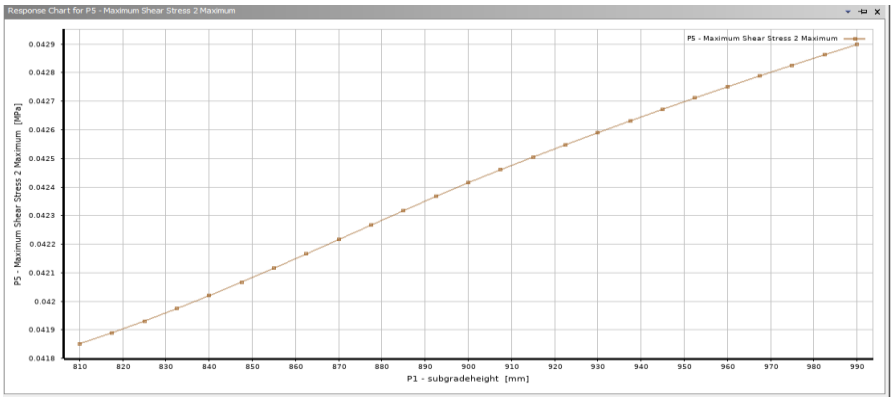

Figure 4.11: Shear Stress v/s Subgrade

The figure depicts the relationship between shear stress and subgrade. The shear stress increases gradually with an increase in the subgrade layer and reaches to the almost maximum stage after 990mm of subgrade thickness. The minimum shear stress was observed for the 810mm subgrade thickness value.

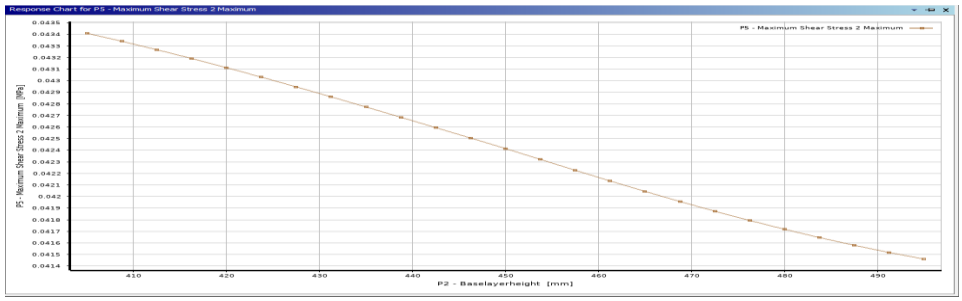

Figure 4.12: Shear Stress v/s Baselayer

The variation of shear stress with respect to base layer is shown in figure. The shear stress decreases gradually with increase in base layer thickness and reaches to minimum value at 495mm of base layer thickness. The maximum shear stress was observed for 405mm base layer thickness value.

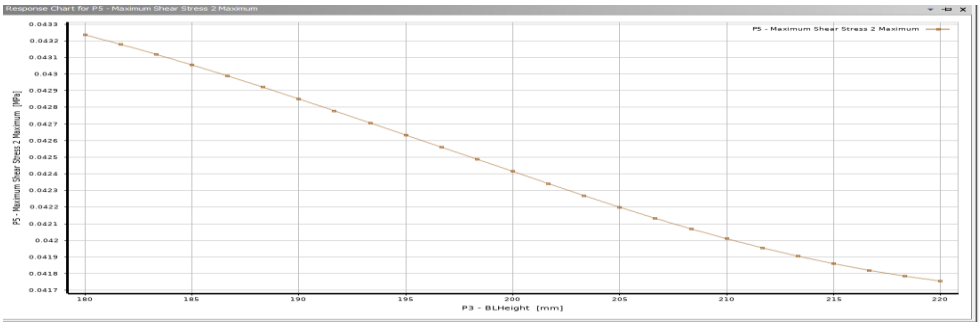

Figure 4.13: Shear Stress v/s Bituminous Layer

The variation of shear stress with respect to the bituminous layer is shown in the figure. The shear stress decreases approximately linearly to reach a maximum value of 220 mm of the bituminous layer.

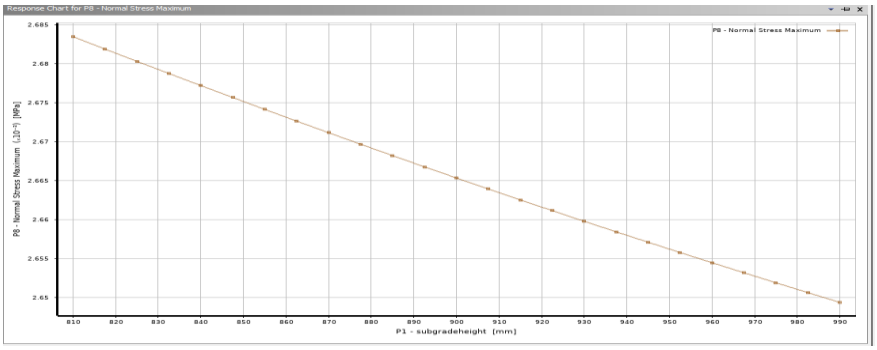

Figure 4.14: Normal Stress v/s Subgrade

The variation of normal stress with respect to subgrade is shown in figure 4.14. The variation of normal stress with respect to subgrade is shown in the figure. The normal stress decreases gradually with an increase in the subgrade layer and reaches to the almost constant stage after 990mm of subgrade thickness. The maximum normal stress was observed for the 810 mm subgrade thickness value.

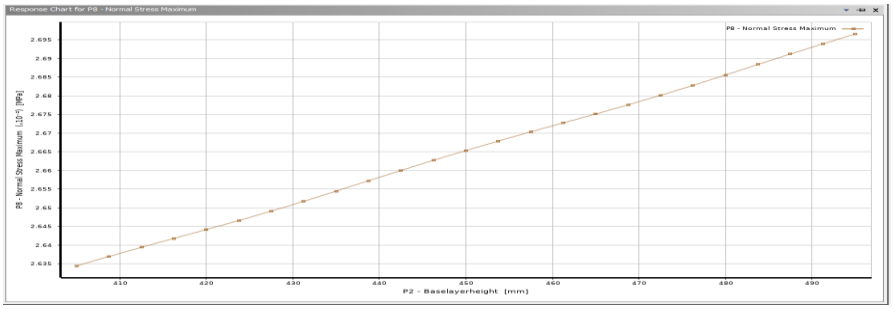

Figure 4.15: Normal stress v/s Baselayer

The variation of normal stress with respect to baselayer is shown in figure 4.15. The variation of normal stress with respect to the base layer is shown in the figure. The normal stress decreases gradually with an increase in base layer thickness and reaches a minimum value of 485mm of base layer thickness.

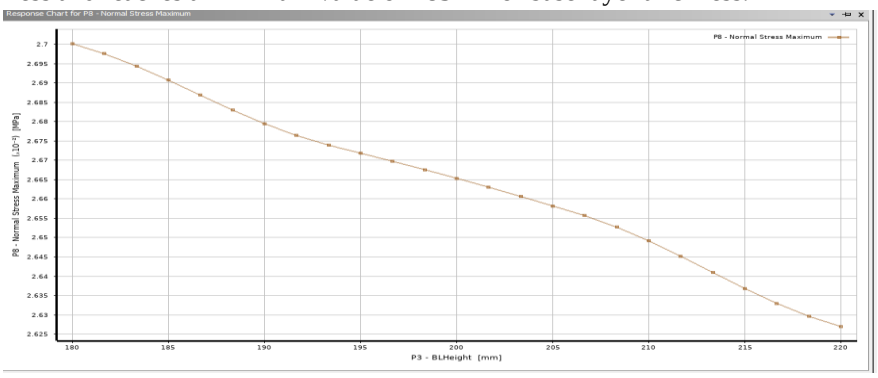

Figure 4.16: Normal Stress vs Bituminous Layer

The figure illustrates the fluctuation in normal stress regarding the bituminous layer parameter. The normal stress decreases with an increase in bituminous layer value and reaches a minimum value of 220mm. The maximum normal stress was observed for a bituminous layer value of 180mm.

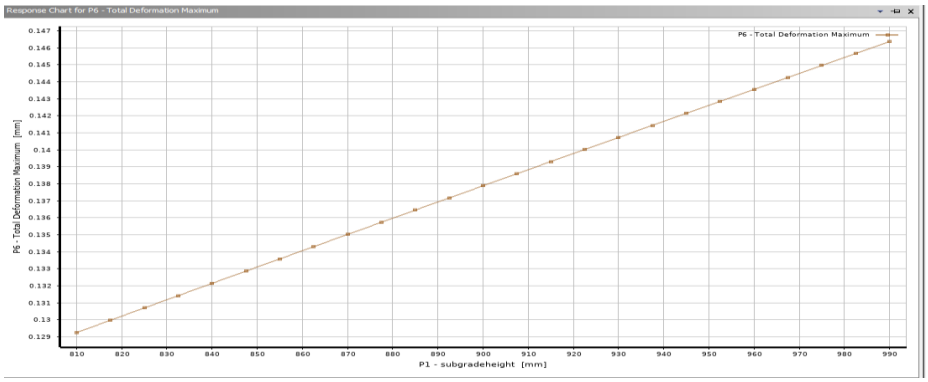

Figure 4.17: Total Deformation v/s Subgrade

Figure 4.17 shows the figure shows the change in total deformation with regard to the subgrade. With increasing subgrade value, overall deformation grows exponentially. A subgrade value of 810mm has the lowest overall deformation, while a value of 990mm has the highest total deformation.

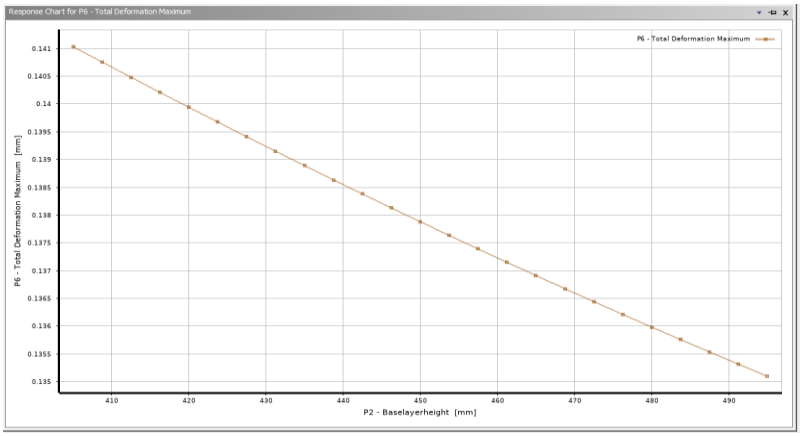

Figure 4.18: Total Deformation v/s Baselayer

The variation of total deformation with respect to the base layer is shown in the figure. The total deformation increases exponentially with an increase in base layer value. The minimum total deformation is observed for a base layer value of 405 mm and the maximum total deformation is observed for a base layer value of 495mm.

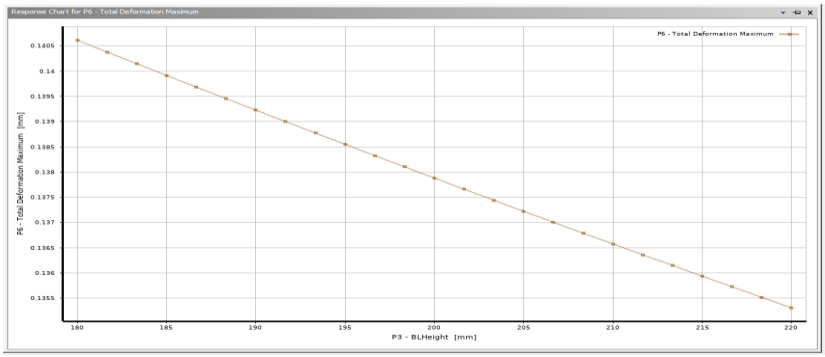

Figure 4.19: Total Deformation v/s Bituminous Layer

Figure 4.19 shows the relationship between total deformation and the bituminous layer. Bituminous layer values decrease linearly in complete deformation. The bituminous layer value of 180mm results in the maximum overall deformation, while the bituminous layer value of 220mm results in the lowest value of total deformation.

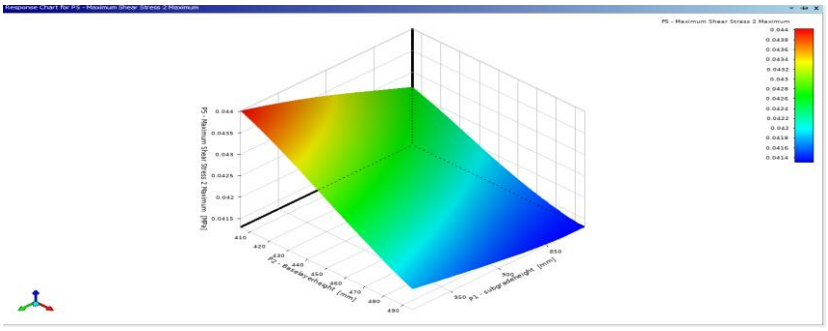

Figure 4.20: Response Surface Plot of Shear Stress

Figure 4.20 shows the figure shows the shear stress response surface plot as it changes over time. The shear stress is greatest for subgrade thicknesses of 920-990mm and for base layer thicknesses of 400-415mm. The shear stress is at its lowest in the dark blue-hued areas displayed.

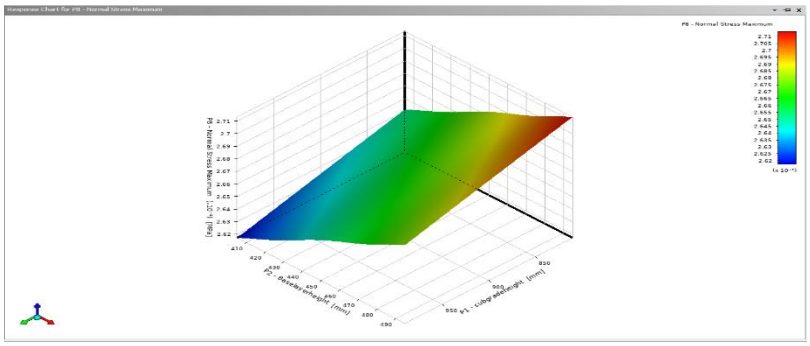

Figure 4.21: Response Surface Plot of Normal Stress

Figure 4.21 shows the usual stress response surface map in 3D. Subgrade values between 800mm and 850 mm and base layer values between 460 and 500 mm provide the highest normal stress on pavement. In the dark blue zone, there is the least amount of usual stress.

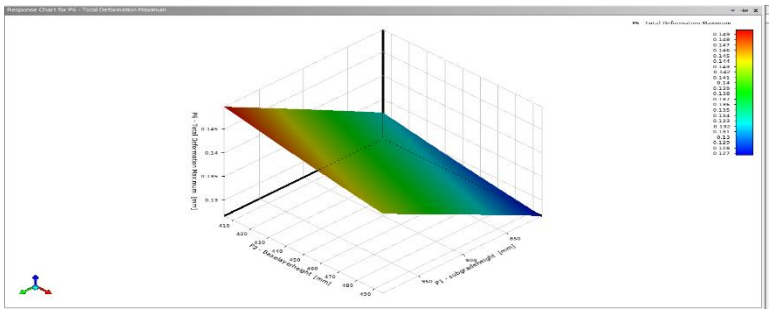

Figure 4.22: Response surface plot of total deformation

Figure 4.22 shows the 3D response surface plot of total deformation. When the subgrade thickness is more than 950mm and the base layer thickness is between 400mm and 470mm, the total deformation of the pavement reaches its maximum. In the dark blue zone, the overall deformation is the lowest.

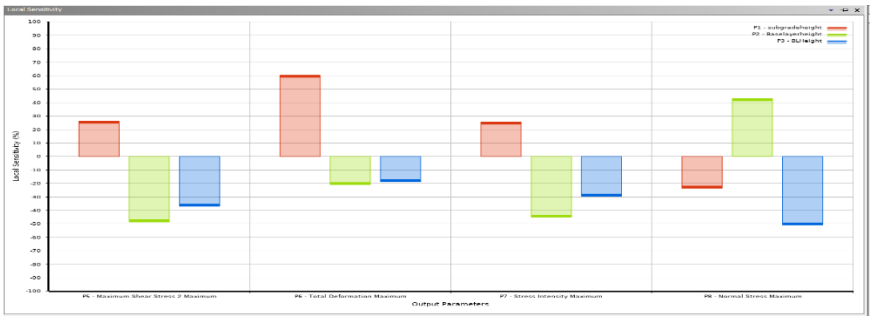

Figure 4.23: Sensitivity Percentage Plot

The Figure 4.23 shows the Sensitivity percentage plots is generated for different variables and output parameters. For shear stress, the subgrade layer thickness has the lowest sensitivity percentage of 26.156% whereas the base layer has the highest sensitivity percentage of 48.678% and the bituminous layer has a sensitivity percentage of 36.989%. The higher sensitivity percentage of the base layer shows that base layer thickness has the highest effect on shear stress.

For normal stress, the subgrade layer thickness has the minimum sensitivity percentage of 23.638% whereas the bituminous layer has the highest sensitivity percentage of 50.762% and the base layer has a sensitivity percentage of 43.116%. The higher sensitivity percentage of the bituminous layer shows that bituminous layer thickness has the highest effect on normal.

For total deformation, the bituminous layer thickness has the lowest sensitivity percentage of 18.703% whereas the subgrade layer has the highest sensitivity percentage of 60.353% and the base layer has a sensitivity percentage of 20.917%. The higher sensitivity percentage of the subgrade layer shows that subgrade layer thickness has the highest effect on total deformation.

5. CONCLUSION AND FUTURE SCOPE

5.1 Conclusion

The results obtained and plots, graphs of different correlation of layers and results of shear stress, normal stress and deformation, I arrived in an outcome.

Finite element-based software tool (ANSYS SOFTWARE) provides a reasonable response and fast analysis and result compared with empirical method of analysis. ANSYS being a user friendly and being a combination of both finite element method and multilayer analysis method, this tool can be effectively used for analysis and design purpose investigating the combined effect of each layer thickness on strength of pavement

The FEA analysis is conducted on pavement to determine the effect of single wheel load on flexible pavement. From the FEA analysis, critical regions of pavement having high normal stress, deformation on flexible pavement is determined. The effect of different pavement layer thickness is then analysed using response method and the findings are summarized below.

1. The minimum shear stress is obtained for design which has dimensions of 826.83mm subgrade and 413.41 base layer and 183.74mm bl.
2. The minimum normal stress is obtained for design which has dimensions of 973.17mm subgrade and 486.59mm base layer and 216.26mm bl.
3. The minimum total deformation is obtained for which has dimensions of 826.83mm subgrade and 413.41 base layer and 183.74mm bl.
4. For shear stress, the higher sensitivity percentage of subgrade layer shows that subgrade layer thickness has highest effect on shear stress.
5. For normal stress, the higher sensitivity percentage of subgrade layer shows that subgrade layer thickness has highest effect on shear stress.
6. For total deformation, the higher sensitivity percentage of subgrade layer shows that subgrade layer thickness has highest effect on shear stress.

5.2 Future Scope

Further analysis can be conducted on pavement by changing material of different layers. The material properties of these layers especially stiffness has significant effect on deformation and normal stress. The use of replacement materials like coal dust, brick dust, replacement aggregates and other coal fly ash, ground granulated blast furnace slag, silica fume, ground glass natural pozzolans or calcined clay (eg, metakaolin).

REFERENCES

[1.] Khan, I.H.(1998) A Textbook of Geotechnical Engineering, Pentice Hall of India Private Limited, New Delhi.

[2.] Arora, K.R. (2003) Soil mechanics and Foundation Engineering, Standard Publishers Distributors, Delhi

[3.] Punmia, B.C., Jain, A.K. and Jain Arun, K.(2005) Soil Mechanics and Foundations, Lakshmi Publications, New Delhi.

[4.] Subagio, B. Cahyanto, H., Rahman, A. and Mardiyah, S.(2005) Multilayer Pavement Structural Analysis Using Method of Equivalent Thickness, Case Study: Jakarta-Cikampeck Toll Road , Journal of the Eastern Asia Society for Transportation Studies, Vol.6,pp.55-65.

[5.] Das, A.(2008) Reliability Considerations of Bituminous Pavement Design by Mechanistic-Empirical Approach, the International Journal of Pavement Engineering, Vol.9, No.1, pp. 19-31.

[6.] Tarefder, R., Saha, N. and Stormont, J.(2010) Evaluation of Subgrade Strength and Pavement Designs for Reliability, Journal Transportation Engineering, Vol.136, No.4, pp. 379-391.

[7.] Rahman, M.T., Mahmud, K. and Ahsan, K. (2011), Stress-Strain Characteristics of Flexible Pavement Using Finite Element Analysis, International Journal of Civil and Structural Engineering, Vol.2, No.1, pp.233-240.

[8.] Ameri, M., Salehabadi, E.G., Nejad, F.M. and Rostami, T. (2012) Assessment of Analytical Techniques of Flexible Pavements by Finite Element Method and Theory of Multi-Layer System, Journal Basic Applied Science Research, Vol.2, No.11, pp.11743-11748.

[9.] Jain, S., Joshi,Y.P., Golia, S.S. (2013) Design of Rigid and Flexible Pavements by Various Methods and Their Cost Analysis of Each Method, International Journal of Engineering Research and Applications, Vol.3, No.5 pp.119-123.

[10.] Dilip, D., Ravi, P. and Babu,G. (2013) System Reliability Analysis of Flexible Pavements, Journal Transportation Engineering, Vol.139, No.10, pp. 1001-1009.

[11.] Maharaj, D.K. and Gill, S. (2014) Development of Design Chart for Flexible Pavement by Finite Element Method, International Journal of Latest Research in Engineering and Computing,Vol.2, Issue 2, MarchApril,pp.8-23.

[12.] Rezaei-Tarahomi, A., Ceylan, H., Gopalakrishnan, K., et al., 2019. Artificial neural network models for airport rigid pavement top-down critical stress predictions: sensitivity evaluation. In: International Airfield and Highway Pavements Conference 2019, Chicago, 2019.

[13.] Kaya, O., Rezaei-Tarahomi, A., Ceylan, H., et al., 2018b. Neural network-based multiple-slab response models for top-down cracking mode in airfield pavement design. Journal of Transportation Engineering, Part B: Pavements 144 (2), 04018009

[14.] Seitllari, A., Kumbargeri, Y.S., Biligiri, K.P., et al., 2019. A soft computing approach to predict and evaluate asphalt mixture aging characteristics using asphaltene as a performance indicator. Materials and Structures 52, 100.

[15.] Moghaddam, T.B., Soltani, M., Shahraki, H.S., et al., 2016. The use of SVM-FFA in estimating fatigue life of polyethylene terephthalate modified asphalt mixtures. Measurement 90, 526e533.

[16.] Tapkin, S., 2014. Estimation of fatigue lives of fly ash modified dense bituminous mixtures based on artificial neural networks. Materials Research 17 (2), 316e325.

[17.] Fakhri, M., Amoosoltani, E., Farhani, M., et al., 2017. Determining optimal combination of roller compacted concrete pavement mixture containing recycled asphalt pavement and crumb rubber using hybrid artificial neural network-genetic algorithm method considering energy absorbency approach. Canadian Journal of Civil Engineering 44 (11), 945e955.

[18.] Liu, T., Zhang, P., Wang, J., et al., 2020b. Compressive strength prediction of PVA fiber-reinforced cementitious composites containing nano-SiO2 using BP neural network. Materials 13 (3), 521.

[19.] Garoosiha, H., Ahmadi, J., Bayat, H., et al., 2019. The assessment of Levenberg-Marquardt and Bayesian framework training algorithm for prediction of concrete shrinkage by the artificial neural network. Cogent Engineering 6 (1), 1609179.

[20.] Dinegdae, Y.H., Birgisson, B., 2018. Effects of truck traffic on topdown fatigue cracking performance of flexible pavements using a new mechanics-based analysis framework. Road Materials and Pavement Design 19 (1), 182e200.

[21.] Liu, Y., Tight, M., Sun, Q., et al., 2019. A systematic review: road infrastructure requirement for connected and autonomous vehicles (CAVs). Journal of Physics: Conference Series 1187 (4), 42e73.

[22.] Xu, Q., 2017. A Potential New Structural Design for Flexible Pavement (Master thesis). Delft University of Technology, Delft.

[23.] Noorvand, H., Karnati, G., Underwood, B.S., 2017. Autonomous vehicles: assessment of the implications of truck positioning on flexible pavement performance and design. Transportation Research Record 2640, 21e28.

[24.] Chen, F., Song, M., Ma, X., et al., 2019. Assess the impacts of different autonomous trucks' lateral control modes on asphalt pavement performance. Transportation Research Part C: Emerging Technologies 103, 17e29.

[25.] Gungor, O.E., Al-Qadi, I.L., 2020. Wander 2D: a flexible pavement design framework for autonomous and connected trucks. Interantional Journal of Pavement Engineering, https:// doi.org/10.1080/10298436.2020.1735636.

[26.] Zhou, F., Hu, S., Xue, W., et al., 2019. Optimizing the Lateral Wandering of Automated Vehicles to Improve Roadway Safety and Pavement Life. Final Report. Texas A&M Transportation Institute, College Station.

[27.] Chen, F., Song, M., Ma, X., et al., 2019. Assess the impacts of different autonomous trucks' lateral control modes on asphalt pavement performance. Transportation Research Part C: Emerging Technologies 103, 17e29.

[28.] M. Avalle, G. Chiandussi, and G. Belingardi, “Design optimization by response surface methodology: application to crashworthiness design of vehicle structures,” Struct. Multidiscip. Optim., vol. 24, no. 4, pp. 325–332, 2002, doi: 10.1007/s00158-002-0243-x.

[29.] A. Y. A. E.-V. Silva, “Utilization of Response Surface Methodology in Optimization of Extraction of Plant Materials,” Rijeka: IntechOpen, 2018, p. Ch. 10.

[30.] M.S. Ranadive, Anand B. Tapase, “Parameter sensitive analysis of flexible pavement” International Journal of Pavement Research and Technology 9 (2016) 466–472